IEEE JOURNAL OF BIOMEDICAL AND HEALTH INFORMATICS

IEEE Xplore® Digital Library
http://ieeexplore.ieee.org/Xplore

Robust Interbeat Interval and Heart Rate Variability Estimation Method from Various Morphological Features using Wearable Sensors

Ayca Aygun, *Student Member*, *IEEE*, Hassan Ghasemzadeh, *Senior Member*, *IEEE*, and Roozbeh Jafari, *Senior Member, IEEE*

***Abstract*— We introduce a novel approach for robust estimation of physiological parameters such as interbeat interval (IBI) and heart rate variability (HRV) from cardiac signals captured with wearable sensors in the presence of motion artifacts. Motion artifact due to physical exercise is known as a major source of noise that contributes to a significant decline in the performance of IBI and HRV estimation techniques for cardiac monitoring in free-living environments. Therefore, developing robust estimation algorithms is essential for utilization of wearable sensors in daily life situations. The proposed approach includes two algorithmic components. First, we propose a combinatorial technique to select characteristic points that define heartbeats in noisy signals in time domain. The heartbeat detection problem is defined as a shortest path search problem on a direct acyclic graph that leverages morphological features of the cardiac signals by taking advantage of the time-continuity of heartbeats – each heartbeat ends with the starting point of the next heartbeat. The graph is constructed with vertices and edges representing candidate morphological features and IBIs, respectively. Second, we propose a fusion technique to combine physiological parameters estimated from different morphological features using the shortest path algorithm to obtain more accurate IBI/HRV estimations. We evaluate our techniques on motion-corrupted photoplethysmogram and electrocardiogram signals. Our results indicate that the estimated IBIs are highly correlated with the ground truth ($r = 0.89$) and detected HRV parameters indicate high correlation with the true HRV parameters. Furthermore, our findings demonstrate that the developed fusion technique, which utilizes different morphological features, achieves a correlation coefficient that is at least 3% higher than that obtained using single physiological characteristic.**

***Index Terms*— Heart Rate, Heart Rate Variability, Interbeat Interval, Motion Artifacts, Physiological Signal Processing, Wearable Sensors.**

I. Introduction

DURING the last decade, cardiovascular diseases (CVDs) have become the leading cause of death worldwide [1]. In 2012, the World Health Organization (WHO) reported an estimated 17.6 million deaths globally due to CVDs, which indicates a significant growth since 2000 [2]. Furthermore, it is estimated that 23.3% of the world population will suffer from cardiac disorders by 2030 [3]. In addition to contributing to increased mortality rates, CVDs also lead to disabilities and decreased quality-of-life [2]. Continuous cardiac monitoring is one of the most essential factors in preventing and managing CVDs. The conventional methods commonly depend on regular hospital visits, which are time-consuming and labor-intensive. In contrast, wearable sensors can provide uninterrupted monitoring, in particular outside clinics, while providing objective assessments of cardiac functions in real-times. This potential of wearable technologies is highly promising especially for conditions where intermittent monitoring is insufficient. However, continuous estimation of the physiological parameters related to CVD from wearable sensors in daily life is very challenging due to disturbances induced by physical motions. To address this challenge, in this article, we aim to develop robust techniques to estimate CVD-related physiological parameters from wearable sensors in free-living environments where various levels of motion artifact are present.

Among various physiological parameters, *heart rate (HR)*, which is the mean value of heart contractions during a fixed time frame, is one of the most significant indicators of cardiac health. Since HR is a key factor in identifying intensity of the physical activities and how body tolerates severe exercises, it is desirable to monitor HR for fitness applications [4]. In addition to HR being an important parameter in assessing cardiac fitness, variations in HR may provide important indications about current cardiac status and related heart diseases [5]. *Heart rate variability (HRV)* is a physiological measure of such variations between consecutive heartbeats. HRV can be measured from *interbeat interval (IBI)* where the IBI itself can be viewed as an estimation of the heart rate during one heartbeat. The variations between adjacent HRs are associated with various physiological

This work was supported, in part by the National Institutes of Health, under grant 1R01EB028106-01, and the National Science Foundation, under grants CNS-1738293 and EEC-1648451. Any opinions, findings, conclusions, or recommendations expressed in this material are those of the authors and do not necessarily reflect the views of the funding organizations.

A. Aygun is with the Department of Electrical and Computer Engineering, Texas A&M University, College Station, TX, 77843 USA (e-mail: aycaaygun@tamu.edu)

H. Ghasemzadeh is with the School of Electrical and Computer Science, Washington State University, Pullman, WA, 99164-2752 USA (e-mail: hassan.ghasemzadeh@wsu.edu)

R. Jafari is with the Department of Biomedical Engineering, Electrical and Computer Engineering, Computer Science and Engineering, Texas A&M University, College Station, TX, 77843 USA (e-mail: rjafari@tamu.edu)

Digital Object Identifier 10.1109/JBHI.2019.2962627

disorders. Therefore, HRV is considered as an important criterion to guide the assessment of cardiac wellness. For example, an infrequent level of fluctuations is a sign of chronic stress [6]. Moreover, HRV is an important benchmark for diagnosis of many medical complications such as cardiac inflammation, anxiety, stress, and sleep quality [6, 7, 8].

Monitoring HR and HRV with wearable sensors in free-living environments is very challenging since these types of sensors are vulnerable to motion artifacts due to body movements (*e.g.,* walking, running). Prior research indicates that capturing HRV from PPG is more challenging than estimating HRV from ECG, mainly because PPG sensors are more sensitive to noise [9]. Specifically, since the pulsatile part of the PPG sensor has quite small amplitude, even moderate physical activities can lead to sliding or rubbing effects on the sensor, which in turn result in an accuracy degradation [10]. Moreover, inappropriate localization of the light-emitting diodes (LEDs) relative to the photodiode (PD) and irregular optical pairings are responsible for introduction of intense noise in wearable sensors [11]. In contrast to HRV, since the average HR is consistent over time while noise is not, it is less challenging to differentiate average HR from noise. There exist several noise reduction techniques in the literature for calculating average HR [12, 13, 14, 15]. However, estimating HRV in the presence of motion artifacts is more challenging due to its inconsistency in the time domain. In fact, HRV and noise are both inconsistent, making it more complicated to detect HRV in the presence of motion artifacts. These challenges raise an unmet need for designing HRV detection algorithms that are robust against the motion artifact.

In this article, we propose a novel technique to estimate IBI and HRV from motion-corrupted PPG and ECG signals with the help of various physiological signal characteristics. A feature extraction technique is used to detect morphological characteristics of different physiological signal modalities such as systolic peaks, maximum slopes, and onsets of PPG signals or R-peaks of ECG signals. A graph model is introduced where the graph vertices and graph edges represent morphological features (*e.g.*, systolic peaks) and IBIs calculated based on those morphological features, respectively. The edge weights in the graph are computed according to the average HR values obtained from a particle filtering technique [12]. Note that any other state-of-the-art methods such as TROIKA and EEMD can be used for the calculation of average HR [13, 14] as our methodologies are independent of the choice of the HR calculation algorithm. The sequential nature of heartbeats is utilized to model the shortest path problem on a direct acyclic graph: "The starting point of one heartbeat is the ending point of the previous one without any discontinuity between the two consecutive heartbeats". A shortest path search problem is introduced to select the best set of heartbeats for robust estimation of IBI/HRV from noisy signals. The objective is to assign the edge weights of the graph effectively so that the most likely edges, *i.e.*, the ones closer to the average IBI, are selected as belonging to the path with the least cost. Furthermore, a fusion technique is introduced for combining the outputs (IBI arrays) of various shortest path calculations, all of which exploit different morphological features of one-channel signal modality, for robust estimation of IBI/HRV in the presence of significant noise levels. To utilize various morphological characteristics of one-channel physiological signals, IBI arrays, which belong to different morphological characteristics, are segmented in time domain and the IBI subarray with less variation is selected from each segment in the light of the fact that the consequent IBIs have small variation in a short period of time. This approach can be viewed as a voting technique, taking the advantage of different characteristics with most agreeable behavior in a certain time period for an accurate estimation of IBI and HRV values.

The main contributions of the proposed work towards accurately estimating IBI and HRV in the presence of motion artifacts can be summarized as follows:

1. A feature extraction technique is used for the detection of the target morphological feature candidates from different physiological signal modalities such as R-peaks of ECG or systolic peaks, maximum slopes, and onsets of PPG.
2. To improve the performance of IBI/HRV estimations in the presence of motion artifacts, the heartbeat selection process is modeled as a shortest path search problem by leveraging the sequential alignments of heartbeats in time domain.
3. A fusion technique is proposed to utilize various morphological features of one type of signal. The outputs (estimated IBI arrays) of separate shortest path calculations, all of which use different physiological characteristics as an input (*e.g.*, systolic peaks or onsets of PPG), are combined to obtain more accurate IBI and HRV.

The reminder of this article is organized as follows. The related works are reviewed in Section II. The physiological signals used in this study along with their characteristics used for IBI detection are introduced in Section III. The details of the proposed method are explained in Section IV. The experimental setup, results, problem complexity, and discussion are presented in Section V. Finally, the conclusion is provided in Section VI.

II. Related Work

There have been numerous methods in the literature that implement various signal processing techniques for robust calculation of average HR from distorted signals. Several recent studies have successfully practiced the estimation of average HR in the presence of intense motion artifacts on the dataset from Signal Processing Cup 2015. This dataset contains noisy signals recorded in the running mode. TROIKA is one of such efforts, which proposes three steps including singular value decomposition (SVD) for removing the out of band noise, sparse signal reconstruction (SSR) to improve the performance of frequency spectrum calculation, and spectral peak selection for estimation of average HR [13]. Robust empirical mode decomposition (EEMD) is another technique for estimating average HR from distorted signals [14]. This method proposes two consecutive stages including ensemble empirical mode

decomposition to decrease the dependence of the algorithm to the former estimated HR values and recursive least squares (RLS) filter to enhance the strength of the algorithm. There have been additional works focus on capturing HR from bio-impedance (Bio-Z) signals. One of them proposes a technique to measure physiological signals by leveraging smart patches which are located in different places on the chest and detect small fluctuations in Bio-Z based on the mechanical changes of heart and lung [16]. Finally, particle filtering, which introduces a recursive technique to estimate the current state of any system, is another method used for HR detection [12]. This technique is based on weighting a set of particles with a prior knowledge and obtaining the posterior probability density of each of the particles to decide the current state of the system (*e.g.*, current heart rate for this case). In the current study, we leverage particle filtering method to acquire the average HR values used as inputs to the proposed algorithm for accurate estimation of IBI and HRV.

There have been relatively few methods on IBI and HRV detection due to the fact that this field of study is rather new. One study aims to calculate IBI with the help of the characteristic locations of a radar signal [17]. Although this method proposes an approach for accurate estimation of IBI, it requires an ultra-wideband radar system equipment, which is not convenient for further development of wearable sensors. Another study introduces the heartbeat detection from motion-artifact-induced PPG signals by leveraging the empirical mode decomposition (EMD) [18]. Although this study provides a technique to discover the peak locations for the estimation of IBI, the motion artifacts due to intense physical activities are not considered. An additional study presents a robust technique for peak selection during intense physical activities by using a personal computer mouse. However, this method still has increased error rates as a result of computer mouse displacements which lead to significant drop in the accuracy [19]. A computer mouse is used as a sensing device.

Another study focuses on HRV detection with the help of off-the-shell smartphones [20]. While this study introduces a robust technique for obtaining HRV parameters for static subjects, it does not provide an approach for noisy conditions. Another method investigates HRV parameters via smartphone PPG [21]. Similarly, this technique does not propose a solution to acquire HRV from motion-disturbed signals, which limits its usability in the development of wearable sensors suitable for everyday life situations. Another study explores the absolute values of the differences between two adjacent IBI values and obtains an optimal threshold to classify the signal epochs as artifacts or non-artifacts [22]. However, this method uses participants in an intensive care unit (ICU) and determines the threshold for this specific dataset, which does not provide a reliable and generalizable technique.

Besides these research efforts, there have been studies that focus on the comparison between the HRV obtained from PPG and ECG signals. One such study examines the statistical comparison between the HRV parameters obtained from handgrip ECG and fingertip PPG simultaneously and reports certain frequency domain HRV parameters [23]. Despite, the results indicate an agreement between HRV parameters obtained from ECG and PPG signals, the experiments do not include motion artifacts. Another method explores the correlations of HRV parameters acquired from ECG and finger-tip PPG signals which are recorded simultaneously [24]. Although this technique reports a high correlation in resting state, again, it does not provide a solution for noisy conditions. There have been also a few investigations to estimate HRV from PPG and HRV from ECG in the presence of motion artifacts. One study proposes a technique to investigate the similarities of HRV parameters obtained from short-term and long-term ECG and PPG readings [25]. Although this study provides accurate results for the comparison, the PPG signal is recorded by using an earlobe sensor which is susceptible to less noise than a wrist-worn PPG due to the higher degrees of movements in the wrist. Another study aims at measuring HRV parameters of ECG signals with an artifact correction technique. This method leverages two variable thresholds where one of them is calculated with the distribution of consecutive IBI differences and the second one is decided with the distribution of differences between particular IBIs and the median IBI [26]. We further investigate the HRV estimation performance of our proposed technique by comparing our results with this artifact correction method.

III. Signal Characteristics

There are different physiological signal modalities such as PPG and ECG that are commonly used to obtain cardiac-related information. Each of these modalities possesses different morphological features such as systolic peak, maximum slope, or onset of PPG and R-peak of ECG. Fig. 1 depicts the signal modalities studied in this article that provide pronounced characteristic points necessary for IBI and HRV estimation. However, our proposed technique is expected to be applicable to other signal modalities leveraging relevant features.

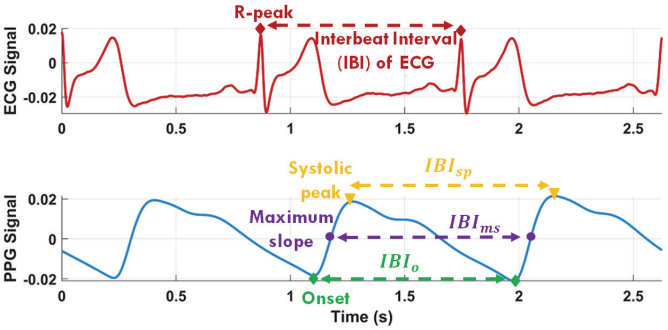

Fig. 1. Different signal types and their representative morphological features

A. Electrocardiogram Signals:

ECG signals capture the electrical activity of the heart and are acquired from the chest with two or more electrodes placed on skin. R-peak is the most pronounced point of an ECG signal and is an evidence of electrical depolarization of the ventricles of the heart. An example of an ECG signal with two R-peaks and an IBI between them is presented in the top graph in Fig. 1. In this work, noisy ECG signals recorded from the chest using wet electrodes are used for the detection of IBI and HRV values.

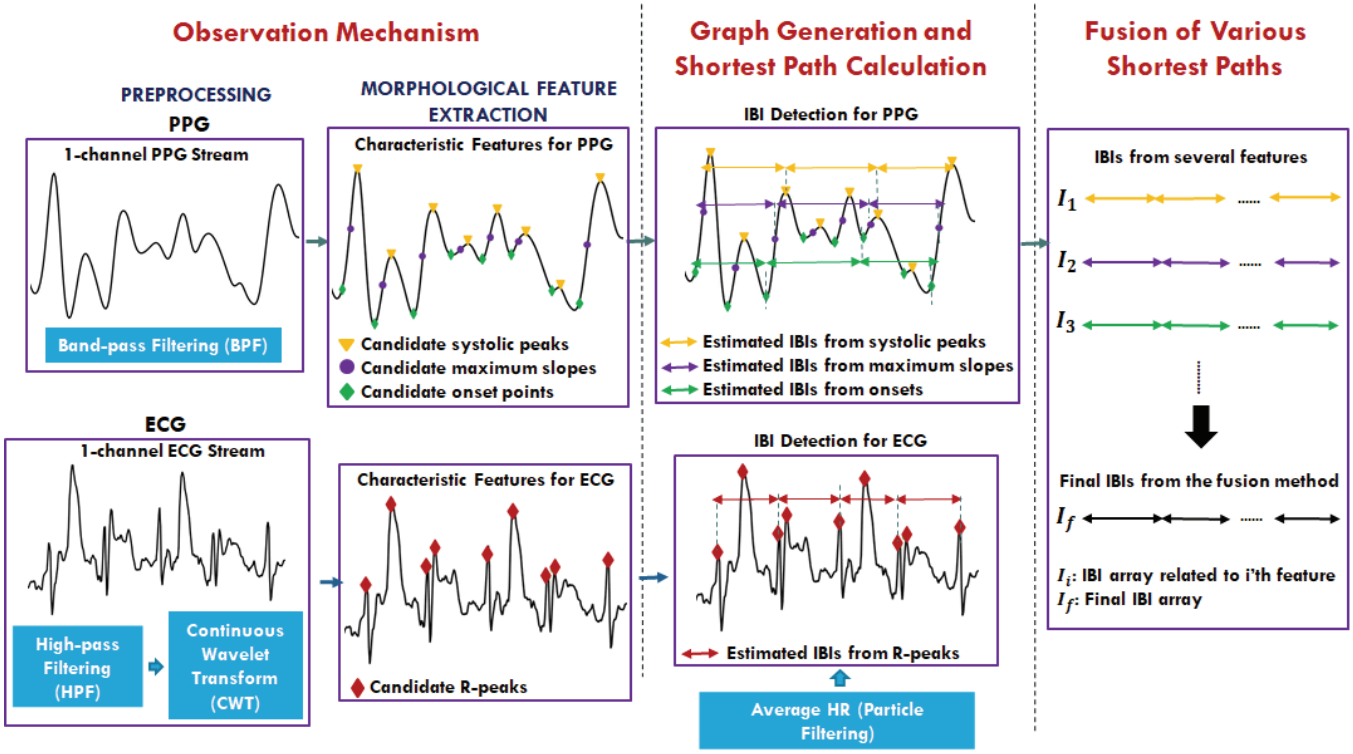

Fig. 2. Overview of the proposed method.

The clean ECG signals are used as a reference for performance evaluation.

B. *Photoplethysmogram Signals:*

PPG signals represent a measure of volumetric changes of heart that can be obtained from transmitted and reflected lights originated from light-emitted diode (LED) source located on the body where arteries are nearby the skin such as fingertips, earlobes, or wrists. In this work, one-channel PPG signal recorded with wrist-worn PPG sensor is used to obtain the IBI and HRV estimations. Three different morphological features (systolic peaks, maximum slopes, and onsets) of PPG are used to estimate the IBI values. An example of a PPG signal with its morphological features is shown at the bottom of Fig. 1. In the figure, IBI_{sp}, IBI_{ms}, and IBI_o represent the IBIs between consecutive systolic peaks, maximum slopes, and onsets, respectively.

IV. Methods

In this work, a robust heartbeat selection technique is proposed to estimate the IBI and HRV from ECG and PPG signals in the presence of motion artifacts. An overview of the proposed method is shown in Fig. 2. First, a morphological feature extraction method is devised to detect the most informative and pronounced characteristic points, such as R-peaks for ECG or maximum slopes for PPG from the motion-distorted ECG and PPG signals. Second, a graph model is introduced to capture relationship between consecutive points on the signal that can be used to compute the IBI values. The problem of selecting the optimal IBI values is modeled as a shortest path exploration problem. The goal of this optimization problem is to determine the most likely heartbeats from the noisy signals and estimate the IBI arrays for each one-channel signal individually where IBI values were estimated from ECG signal leveraging this technique in our previous work [27]. Finally, a novel fusion technique is introduced to utilize different morphological features of one-channel signal to accurately infer IBI and HRV. Note that although the proposed fusion technique can be applied to different signal modalities such as PPG and ECG to utilize various characteristic features, in this paper we use our fusion technique to combine different morphological features and estimate IBI and HRV from merely PPG signals. This has been done to investigate the reliability of the proposed method in estimating IBI and HRV from wrist-worn sensors and smartwatches that are only equipped with PPG sensors.

A. *Observation Mechanism*

Observation mechanism includes preprocessing and morphological feature extraction from each signal modality including PPG and ECG that will be explained in detail in the following two sections.

Preprocessing

First, the ECG and PPG signals are upsampled from 125 Hz to 500 Hz to provide a better resolution in IBI estimation. The upsampling will help us to capture the time features in the corresponding signals more accurately. It is also important to note that most important signal information resides in much lower frequencies, in the range of 0-10 Hz [21]. Then, the noisy PPG signals are filtered using a bandpass Butterworth filter with cutoff frequencies of 0.5 Hz and 15 Hz to eliminate unwanted frequency components. Furthermore, the noisy ECG

signals are passed through high-pass Butterworth filters with a cutoff frequency of 0.5 Hz, and continuous wavelet transform (CWT) is used by applying the Mexican hat wavelet with a center frequency of 0.25 Hz. This approach accentuates R-peaks and diminishes other non-R-peaks [12].

Morphological Feature Extraction:

We start by extracting morphological features of one cardiac cycle from each signal modality that correspond to heart activities. In this work, systolic peaks, maximum slopes, and onsets for PPG and R-peaks for ECG are used as the morphological characteristic points of the signals. These feature points are utilized to estimate the interbeat intervals in the light of the fact that interbeat interval is an effective criterion to do a comparison among various signal modalities such as ECG and PPG which occur in one cardiac period [28]. The QRS complex, which represents the ventricular depolarization of the heart, is the strongest component of an ECG signal where R-peak is the most remarkable feature of a QRS complex and can be used to define heartbeats [29]. Moreover, systolic peaks, maximum slopes, and onset points are important characteristics to determine any cardiac cycle of a PPG signal all of which are included in the anactoric phase (the systolic phase) of one cardiac period and associated with the contraction of the heart [30, 31]. These morphological characteristics have essential roles of diagnosing cardiac related diseases. For example, R-peak detection has a significant role of detecting heartbeat irregularities, systolic peak estimation is beneficial to estimate large-artery damage and stroke volume, and maximum slope of a PPG was reported as highly correlated with systolic blood pressure [32, 33, 34]. Moreover, onset point of a PPG is an important feature to extract cardiac activity which is less affected of distortions and baseline variations as well as it is an important benchmark to assess pulse transit time and pulse wave velocity where these indicators are utilized to detect the impacts of aging, hypertension, stiffness, and atherosclerosis [35]. There have been additional studies investigate various physiological parameters extracted from Bio-Z signals to be used for the estimation of physiological measures such as blood pressure [36].

Systolic peak candidates of PPG and R-peak candidates of ECG are determined leveraging a peak selection process which detects the local maxima of PPG and ECG signals, respectively. To decide the candidate maximum slopes, the peaks of the first derivative of the PPG are detected as shown in Fig. 3. The strongest peaks of the first derivative, (shown in the middle of Fig. 3) are used as the maximum slopes as suggested in [37]. The second derivative of the PPG is used to detect the candidate onsets of the noisy PPG. The peaks of the second derivative correspond to the onsets of PPG (shown at the bottom of Fig. 3) [30, 35, 38]. The first and second order derivatives are calculated using Savitzky-Golay method [39].

The time difference between two consecutive same features can be considered as the IBI; however, in the presence of motion artifacts, there will be many false features detected from the distorted signal. These false detections will lead to large errors in the IBI calculation. To deal with this problem, the candidate feature sets are used to generate a graph and subsequently a shortest path is calculated to capture the best set of heartbeats. The shortest path is calculated for each feature separately for each signal channel.

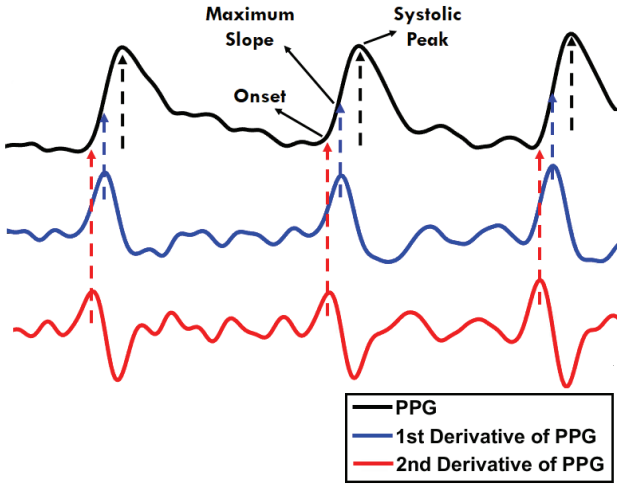

Fig. 3. PPG Signal with its 1st and 2nd order derivatives representing the maximum slopes and onsets of PPG, respectively.

B. Graph Modeling and Heartbeat Detection

A weighted graph is constructed to detect true set of IBI sequences using features extracted from the motion distorted signals. Note that some of the features incorrectly characterize heartbeats and IBIs due to the motion artifacts. In the graph, the vertices represent characteristics and morphological features (*e.g.*, all possible choices of systolic peaks of one-channel PPG) while the edges correspond to candidate IBIs, *i.e.,* the time differences between these morphological features. The sequential alignment of the heartbeats motivates the formation of a path in the graph model. The starting point of one heartbeat is the ending point of the previous one and there is no discontinuity between them, and hence if a path that satisfies

TABLE I
NOTATIONS

Term	Description
v_i	i'th vertex
V	Set of all of the vertices
N	Number of vertices
N_i	Set of the former vertices of i'th vertex
m_i	Number of former vertices of i'th vertex
e_{ij}	Edge (time difference) between i'th and j'th vertices
w_{ij}	Weight of the edge e_{ij}
w_i	Weight of the i'th vertex
t_i	Time length for i'th vertex to choose its former vertices
$(IBI_{avg})_i$	Average IBI of the window that centers the i'th vertex
pn_i	Chosen previous vertex of i'th vertex
V_{chosen}	The set of chosen vertices
I_i	IBI set of i'th feature
I_{ij}	j'th segment of I_i
n_{ij}	Number of elements of I_{ij}
i_{ij}^k	k'th element of I_{ij}
SD_{ij}	Standard deviation of the elements of I_{ij}
s_j	Index of the IBI array selected for j'th segment
I_F	Final IBI set
f	Number of features belong to one-channel stream

certain criteria meeting concerning the average HR is determined, that could represent the sequence of IBIs.

The details of graph generation and the shortest path calculation are presented in Algorithm I. The notations related to the algorithms are illustrated in Table I. The set of vertices of the graph is defined as follows:

$$V = (v_1, v_2, \dots, v_N) \quad (1)$$

where N is the number of all vertices. Each vertex except v_1 could be connected to all the possible former vertices. The vertices connected to any vertex v_i are chosen within a window of length t_i around v_i as shown in Fig. 4-a. We calculate the weight of the edges based on the average IBI. The average IBI is given by:

$$(IBI_{avg})_i = \frac{60000}{(HR_{avg})_i}[ms] \quad (2)$$

$$t_i = (IBI_{avg})_i \times \alpha \quad (3)$$

where $(IBI_{avg})_i$ denotes the average IBI of the i'th vertex and is calculated from $(HR_{avg})_i$, which represents the average heart rate related to the i'th vertex obtained from the particle filter approach [12]. t_i is the time interval specified for each vertex for the selection of the neighboring vertices eligible for establishing edges. α is used to define t_i proportional to related average IBI for the selection of vertices connected to each vertex within a time interval close to average IBI. α is empirically determined through our experiments and is set to 1.5. We observe that, in the case of less noisy signals, the performance improves as α is decreased due to the fact that the morphological features can be detected more accurately in the presence of less motion artifacts and even smaller t_i values might possibly include the correct characteristic points (vertices). However, it will be more difficult to determine morphological features in the presence of intense motion artifacts, therefore, we need larger t_i to increase the chance of detecting the features that correspond to true heartbeats. The average HR values are obtained separately for 8-sec windows that are centered around each vertex or corresponding characteristic points. The intuition behind this approach for choosing the former vertices is the fact that despite the HR variations from one beat to another, the period corresponding to heartbeats always remain close to the average HR. The former vertices set for vertex v_i is then defined as follows:

$$N_i = \{v_{i-m_i}, \dots, v_{i-1}\} \quad (4)$$

where m_i denotes the number of former vertices of the i'th vertex. The most likely candidate former vertices are chosen as the ones close to $(IBI_{avg})_i$with a tolerance of ε. Then, the weight of the edge connecting vertex v_i to its former vertex v_j is calculated using the equation below:

$$w_{ij} = e^{\min\left(\left|(IBI_{avg})_i - \varepsilon - e_{ij}\right|, \left|(IBI_{avg})_i + \varepsilon - e_{ij}\right|\right)} \quad (5)$$

where $e_{ij} = v_i - v_j$ is the time difference between i'th and j'th vertices. If the edge lies within the range of $(IBI_{avg})_i \overline{+/-}\, \varepsilon$, the weight is defined as zero as illustrated in Fig. 4-b; otherwise, the weight w_{ij} is proportional to the distance of vertex v_j from $(IBI_{avg})_i$. The intuition behind this weighting function is the fact that the true IBIs should remain close to the average IBI calculated from the average HR with a preset tolerance and the ones outside of this region should be penalized. Through the shortest path calculation, we ensure that the set of selected heartbeats minimize the total penalty of IBIs that do not meet the distance criteria from the average IBIs calculated from the average HR.

The weights of vertices are calculated by using the weights of the edges between the vertex and its former vertices as shown in Fig. 4-c, based on the following equation:

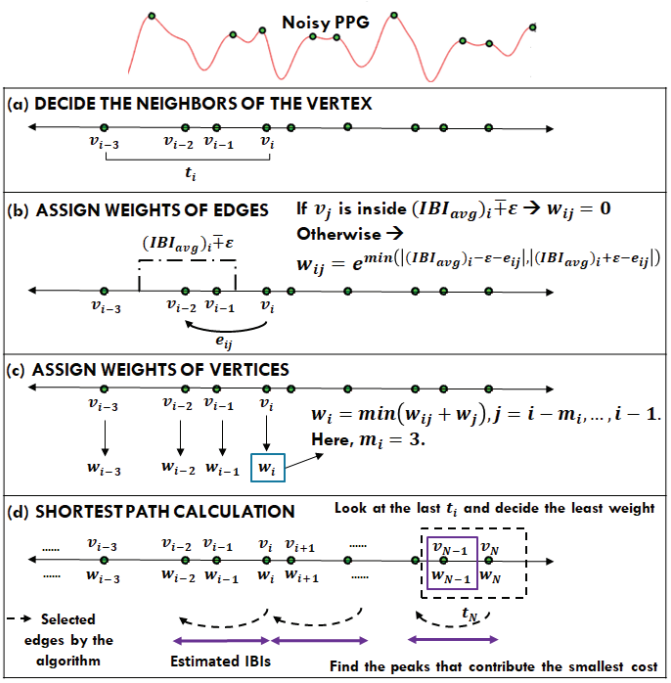

Fig. 4. The process of graph generation and shortest path calculation for choosing true IBIs.

Algorithm I: Shortest Path Modeling, Cost Assignment and Shortest Path Detection

Input: All the feature candidates from a single-channel stream
Output: V_{chosen} the set of all chosen vertices

1. **for** $i = 2$ to N **do** // Calculate the weights
2. **for** $j = i - m_i$ to $i - 1$ **do** // m_i is the number of former vertices of v_i ($m_i < i$)
3. Calculate w_{ij} // using Equation 5
4. **end for**
5. $w_i = min(w_{ij} + w_j)$ // for $j = i - m_i, \dots, i - 1$
6. $pn_i = \underset{v_j \in N_i}{argmin}(w_{ij} + w_j)$ // N_i is the set of former vertices of v_i, and pn_i is the chosen previous vertex for v_i that contributes minimum accumulated weight for vertex v_i
7. **end for**
8. $(v_{N-m_N}, \dots, v_{N-1}, v_N)$ // The last set of vertices
9. $v_{chosen} = \underset{v_k}{argmin}(w_N, w_{N-1}, \dots, w_{N-m_N})$ // The smallest accumulated distance in the last time interval t_N where $k = N - m_N, \dots, N-1, N$.
10. $V_{chosen} \leftarrow v_{chosen}$ // v_{chosen} is the chosen last vertex
11. **for** $k = N$ to 1 **do** // Backward search
12. **if** $v_{chosen} == v_k$ **do**
13. $v_k = pn_k$
14. **end if**
15. $V_{chosen} \leftarrow v_k$ // Push v_k into V_{chosen}
16. **end for**

$$w_i = \min\left(w_{ij} + w_j\right), j = i - m_i, \dots, i - 1. \quad (6)$$

The former vertex prior to v_i which contributes the minimum weight w_i is chosen as follows:

$$pn_i = \underset{v_j \in N_i}{argmin}(w_{ij} + w_j) \quad (7)$$

The vertex with the minimum accumulated weight, is picked inside t_N as illustrated in Fig. 4-d.

This method enables detection of the path with the smallest weight for the robust selection of most likely IBIs that are closer to average IBIs. We refer to the set of all predicted IBIs by Algorithm I as IBI array.

C. *Fusion of Various Shortest Paths*

One IBI array is generated per each morphological feature of each channel of PPG or ECG signals by applying the aforementioned shortest path algorithm. However, in the presence of intense motion artifacts, IBIs can be estimated differently for various parts of the signal due to the imprecise extraction of morphological feature candidates from motion noise contaminated signals. Therefore, we need to develop a technique to combine IBI arrays obtained from various morphological features in case they present diverse estimated IBIs for the same heartbeats.

Assume that IBI arrays, obtained from different shortest path calculations (by leveraging various features), are denoted by I_i where $i = 1,2, \dots, f$ where f indicates the number of features. First, all of the IBI arrays are divided into p segments. We then select the corresponding IBIs per segment for each IBI array, and consider a voting tactic among several IBI arrays for a fixed time period to determine the most consistent reported IBIs. The collective IBI arrays are denoted by the combination of segments as follows:

$$I_i = \bigcup_{j=1}^{p} I_{ij} \quad (8)$$

where I_{ij} indicates the j'th segment of the array I_i. In the above of Fig. 5, rows depict IBI arrays corresponding to various features and columns correspond to different segments.

Algorithm II: Fusion Method to Utilize Various Shortest Paths for Single Stream

Input: I_i the IBI set calculated from the i'th feature of the stream where $i = 1,2, \dots, f$.
Output: The final IBI set: I_F = [].

1. **for** $j = 1$ to p **do** // Dividing IBI arrays into p segments
2. $I_{ij} = \left\{i_{ij}^1, i_{ij}^2, \dots, i_{ij}^{n_{ij}}\right\}$ // IBIs of each segment
3. Decide the length of the segment by using the first IBI array I_{1j} as a base
4. Calculate SD_{ij} // Standard deviation of each segment
5. $s_j = \underset{i}{argmin}(SD_{ij})$ // Find the IBI array related to the corresponding segment that has the smallest standard deviation
6. $I_{s_j j} = \left\{i_{s_j j}^1, i_{s_j j}^2, \dots \dots, i_{s_j j}^{n_{s_j j}}\right\}$
7. **for** $k = 1$ to $n_{s_j j}$ **do** // Update the IBI lengths of $I_{s_j j}$ by normalizing them with respect to the length of I_{1j}
8. $i_{s_j j}^k = \frac{I_{s_j j}^k}{\sum_{l=1}^{n_{s_j j}} I_{s_j j}^l} \times I_{1j}$
9. **end for**
10. $I_F \leftarrow I_{s_j j}$
11. **end for**

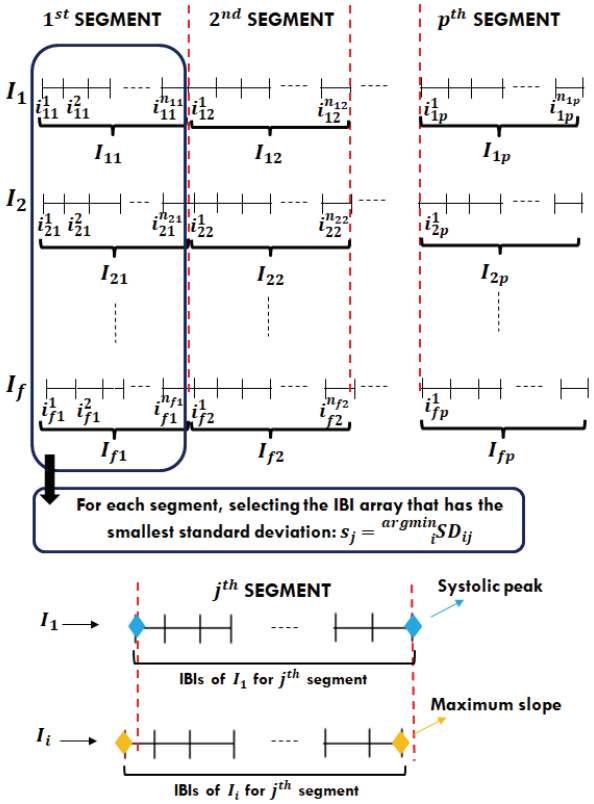

Fig. 5. The fusion technique to utilize various morphological features. The segmentation process is shown at the top of the figure and the identification of the starting and ending points of each segment is indicated at the bottom of the figure.

To perform the segmentation, I_1 is divided into several pieces all of which contain fixed number of consecutive IBIs – empirically defined as 10 for this work. These time pieces of I_1 are stored as a reference to guide segmentation of other IBI arrays to establish correspondence. First, we record the starting and ending points of each segment of I_1 – the starting feature point of its first IBI and the ending feature point of its last IBI. At the bottom of Fig. 5, one segment is shown for two different feature arrays I_1 and I_i which are assumed to represent systolic peaks and maximum slopes, respectively. As seen in the figure, the starting and ending points of the segment is determined with the feature points (systolic peaks) of I_1. As each IBI array represents a particular morphological feature, the second step is to identify the characteristic points of other IBI arrays which correspond to those feature points at the starting and ending points of the segments of I_1 previously recorded in the first step by ensuring that they belong to the same heartbeat. At the bottom of Fig. 5, the systolic peaks at the starting and ending points of the j^{th} segment of I_1 are used to determine the feature points (maximum slopes) of I_i where the systolic peaks at the boundaries of the segment of I_1 and the selected maximum slopes of I_i belong to the same heartbeat. After detecting the feature points of each IBI array that correspond to the starting and ending points of the segments of I_1, the third step is to select the IBIs of the segments for each IBI array. Despite the

segregating nature of our segmentation process with respect to isolating the feature arrays, we maintain the sequential alignment of consecutive IBIs since the starting and ending feature points of the segments from each IBI array belong to the same heartbeat.

Then, for each segment, the standard deviation is calculated for all IBI arrays and the array with the smallest standard deviation is selected as the winning segment:

$$s_j = \underset{i}{argmin}(SD_{ij}) \quad (9)$$

In Equation 9, SD_{ij} is the standard deviation of IBIs included in I_{ij} and s_j is the index of the IBI array which is selected for j'th segment. We chose the standard deviation to select the proper IBI array (morphological feature) for each segment based on the assumption that the variation of IBIs in a short period of time from more precise segment is expected to be smaller. The final IBI array is defined as the combination of the selected IBI arrays for each segment as follows:

$$I_F = \bigcup_{j=1}^{p} I_{s_j j} \quad (10)$$

Algorithm II provides the details of our fusion technique. In the current work, one morphological feature (R-peak) of ECG and three different morphological features (systolic peak, maximum slope, and onset) of PPG are used for IBI and HRV estimation. For PPG signals, the fusion method is applied to three IBI arrays which are obtained from three shortest paths acquired from the three features.

V. Experimental Results

The objective of this study is to estimate IBI and HRV from different physiological signal modalities in the presence of intense motion distortions. We evaluate the performance of our algorithm on ECG and PPG signals corrupted with various levels of noise. In this section, first we introduce the dataset used to test our techniques. Then, we define the evaluation criteria and present the results of IBI estimation with various noise levels to assess the performance of our techniques. We will also analyze various HRV parameters obtained from noise contaminated ECG and PPG signals and provide a comparison to the reference HRV parameters.

A. Dataset

To evaluate the performance of our techniques, we used a dataset from the IEEE Signal Processing Cup 2015 which includes two-channel PPG signals, a three-axis accelerometer (ACC), and a one-channel ECG signal recorded simultaneously at a sampling rate of 125 Hz from 12 subjects aged between 18 and 35 [13]. A wrist-worn dual PPG sensor leveraging green LEDs with two sensors placed at a distance of 2 cm was used to record PPG signals while the three-axis acceleration signals were acquired from a wrist worn ACC sensor. The ECG signal was also recorded with wet ECG electrodes placed on the chest. The duration of all the recordings are 5 minutes. Two experimental scenarios were designed and implemented as shown in Table II, where subject 1 participated in the Scenario 1 and all the remaining subjects participated in Scenario 2.

As the Signal Processing Cup 2015 dataset contains only clean ECG, we need a mechanism to generate a motion-corrupted ECG signal to evaluate the performance of our algorithm on noisy ECG. To obtain a real motion artifact noise, we leveraged the MIT-BIH Noise Stress Test dataset [40, 41]. This dataset, which include motion artifact signals, provides the ability to add realistic motion artifact to clean ECG signals. We created motion artifacts corresponding to five different SNR levels (6dB, 4dB, 2dB, 0dB, and -2dB), and added them to the clean ECG signals to produce noisy ECG signals. The clean ECG signals of the Signal Processing Cup 2015 dataset are used as the ground truth for the performance evaluation.

TABLE II
Experimental Scenarios

Scenario 1 - Rest (30 s) → 8 km/h (1 min) → 15 km/h (1 min) → 8 km/h (1 min) → 15 km/h (1 min) → Rest (30 s)
Scenario 2 - Rest (30 s) → 6 km/h (1 min) → 12 km/h (1 min) → 6 km/h (1 min) → 12 km/h (1 min) → Rest (30 s)

B. Interbeat Interval Results

To investigate the performance of our technique, we analyze the agreement between estimated and true IBI arrays with the help of the Pearson correlation.

Interbeat Interval Acquired from ECG

To demonstrate the robustness of our technique in detecting IBIs leveraging the shortest path algorithm, the correlations between the estimated and true IBI arrays are calculated at five different motion distortion levels for ECG. Table III depicts the Pearson correlation coefficients obtained from 12 subjects in the presence of five different SNR levels. As seen in Table III, the mean of the correlation coefficients between the estimated and true IBI arrays are 0.960, 0.948, 0.939, 0.910, and 0.837 for the SNR levels of 6dB, 4dB, 2dB, 0dB, and -2dB, respectively. The means of the correlation coefficients are above 0.90 while the SNR levels are 6dB, 4dB, 2dB, or 0dB. Although, the correlations between estimated and true IBI arrays decrease when the SNR is decreased gradually, the Pearson correlation coefficients hover around 0.90 for most of the subjects separately even at 0dB SNR. However, the correlation results are relatively worse for subject 11 compared to the rest of the subjects due to the fact that the average HR

TABLE III
IBI Estimation Performance For Noisy ECG in Different SNR Levels

Subject	r (6 dB)	r (4 dB)	r (2 dB)	r (0 dB)	r (-2 dB)
1	0.993	0.986	0.979	0.947	0.903
2	0.989	0.974	0.950	0.909	0.834
3	0.989	0.985	0.975	0.929	0.899
4	0.999	0.983	0.975	0.951	0.940
5	0.997	0.940	0.904	0.887	0.770
6	0.979	0.974	0.986	0.982	0.923
7	0.948	0.952	0.955	0.904	0.750
8	0.999	0.984	0.933	0.897	0.800
9	0.997	0.980	0.964	0.940	0.910
10	0.936	0.977	0.965	0.932	0.788
11	0.716	0.707	0.745	0.771	0.662
12	0.980	0.936	0.940	0.870	0.859
Average	0.960	0.948	0.939	0.910	0.837

values, which are obtained from an existing state-of-the-art technique and used for weight assigning of the edges in the graph model, are relatively worse for this subject which leads lower estimation performance. Moreover, we observe that the correlations between estimated and true IBI arrays decrease significantly when the SNR is -2dB due to the fact that in the presence of intense noise, the error rates of average HR increases which affects the IBI estimation performance. The dependence of our technique to average HR values is discussed in detail in Section V-E.

Interbeat Interval Acquired from Fusion of PPG Features

To evaluate the performance of our IBI detection as well as fusion technique, we estimate IBI by using the fusion technique applied to three different morphological features of PPG signals: systolic peaks, maximum slopes, and onsets as explained in Section IV-A. To demonstrate the effectiveness and the importance of the feature fusion technique (Section IV-C), we estimate the IBI arrays with the usage of each morphological feature individually, with the fusion of any two of them, and with the fusion of all of the morphological features together and investigate the performance of our algorithm. Fig. 6 presents the mean values of the correlation coefficients between the estimated and true IBI arrays for 12 subjects. In this figure, f_1, f_2, and f_3 represent systolic peaks, maximum slopes, and onsets of PPG signal features, respectively, while the summation of them indicates their usage together. The correlation coefficient results indicate that fusions of any of the two morphological features provide higher correlation between the estimated and the true IBI arrays compared to leveraging the features individually. Moreover, the fusion of all the three morphological characteristics has the highest mean of the correlation coefficients which is around 0.89. Leveraging the fusion technique and all three morphological features, the mean of the correlation between the estimated and the true IBI arrays increases at least more than 3% compared to the case of using any single morphological feature and the difference is around 7% in the case we use systolic peaks only.

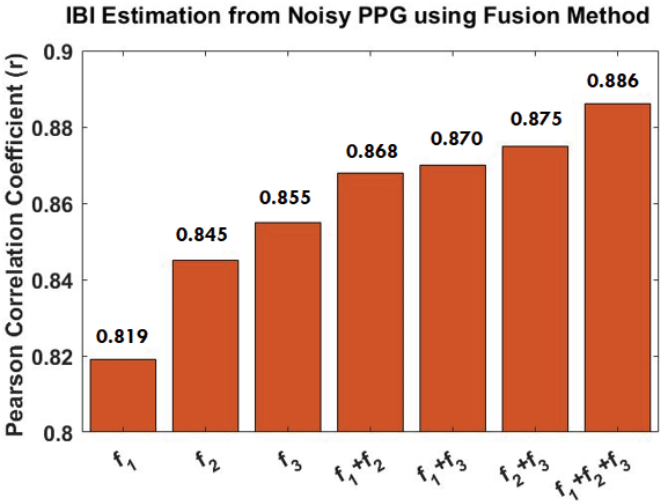

Fig. 6. Pearson correlation coefficients corresponding to the usage of the features $f1$ (systolic peaks), $f2$ (maximum slopes), $f3$ (onsets) individually, fusion of any of two features, and fusion of all of three features.

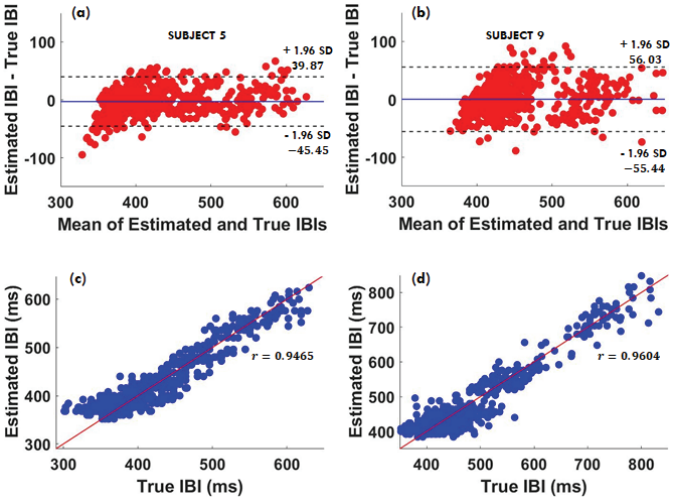

Fig. 7. Bland-Altman plots (a-b) and Pearson plots (c-d) of IBIs for selected subjects obtained the fusion technique from noisy PPG signals.

Moreover, the Bland-Altman plots of the estimated IBI obtained from noisy PPG leveraging all three morphological features and the true IBI obtained from clean reference ECG are shown in Fig. 7 (a-b) for selected subjects which illustrates a high correlation. The 95% limits of agreements are $[39.87, -45.45]$ ms and $[56.03, -55.44]$ ms for subject 5 and subject 9, respectively. Although, the 95% limits of agreement are reported around ∓ 35 ms in some previous works, the experiments of these techniques are done in resting state or less noisy conditions which is the possible reason of relatively lower values [24, 42]. Moreover, the Pearson correlation plots are shown in Fig. 7 (c-d) with the Pearson correlation coefficients of 0.9465 and 0.9604 illustrates that the estimated IBI array from noisy PPG is highly correlated with the ground truth.

We further evaluate the performance of our fusion technique by comparing the original ACC and PPG signals. Fig. 8 (a) and (b) shows the spectrogram of an ACC signal and the spectrogram of a PPG signal with the true HR, respectively. The figures demonstrate that acceleration components are contaminating PPG signals as well and there is a high correlation between the original ACC and PPG signals. The frequency component corresponding to the the true heart rate however is also visible and is quite different from the stepping rate. Moreover, to demonstrate how much enhancement our proposed technique provides in terms of the IBI estimation in comparison with the most rudimentary technique, Fig. 8 (c) presents the true IBI, the estimated IBI obtained from our fusion method, and the estimated IBI obtained with Eq. 2. The results indicate that our proposed technique provides an accurate IBI estimation from noisy PPG signals.

C. *Heart Rate Variability Results*

We evaluate the performance of our techniques in estimating the HRV parameters from noisy ECG and PPG signals in this section. The estimated IBI arrays are used as an input to Kubios software that can calculate different HRV parameters [43]. Eight HRV parameters are obtained from the estimated and the true IBI arrays for 12 subjects. Four time-domain parameters include the mean IBI (ms), the SDNN (standard deviation of

TABLE V
HRV COMPARISON RESULTS FOR NOISY ECG IN VARIOUS SNR LEVELS

HRV Parameters	Mean RR (*ms*)	SDNN (*ms*)	Mean HR (*1/min*)	STD. HR (*1/min*)	LF Power (ms^2)	HF Power (ms^2)	VLF Power (ms^2)	Total Power (ms^2)
Our Method (6 dB)	0.999	0.997	0.999	0.996	0.978	0.950	0.999	0.998
Lipponen et. al. (6 dB)	0.998	0.988	0.997	0.967	0.998	0.989	0.967	0.972
Our Method (2 dB)	0.999	0.993	0.999	0.997	0.859	0.863	0.998	0.988
Lipponen et. al. (2 dB)	0.995	0.984	0.994	0.969	0.859	0.765	0.966	0.975
Our Method (-2 dB)	0.998	0.970	0.999	0.954	0.613	0.746	0.976	0.886
Lipponen et. al. (-2 dB)	0.881	0.846	0.900	0.475	0.578	0.722	0.847	0.898

IBI in ms), the mean HR ($1/min$), and the STD HR (standard deviation of HR in $1/min$) and four others are frequency domain parameters namely the LF power (low frequency power in ms^2), HF power (high frequency power in ms^2), VLF power (very low frequency power in ms^2), and the total power (ms^2). Studies indicate that time domain HRV parameters provide a valuable information to determine the patterns of heart rate regulation during reperfusion besides frequency domain HRV parameters carry beneficial information to estimate the fluctuations in HRV during myocardial ischemia [5]. More specifically, HF is an important benchmark to assess the respiratory patterns and LF carries significant information related to blood pressure control, peripheral vasomotor activity, and sympathetic outflow [5, 42, 44].

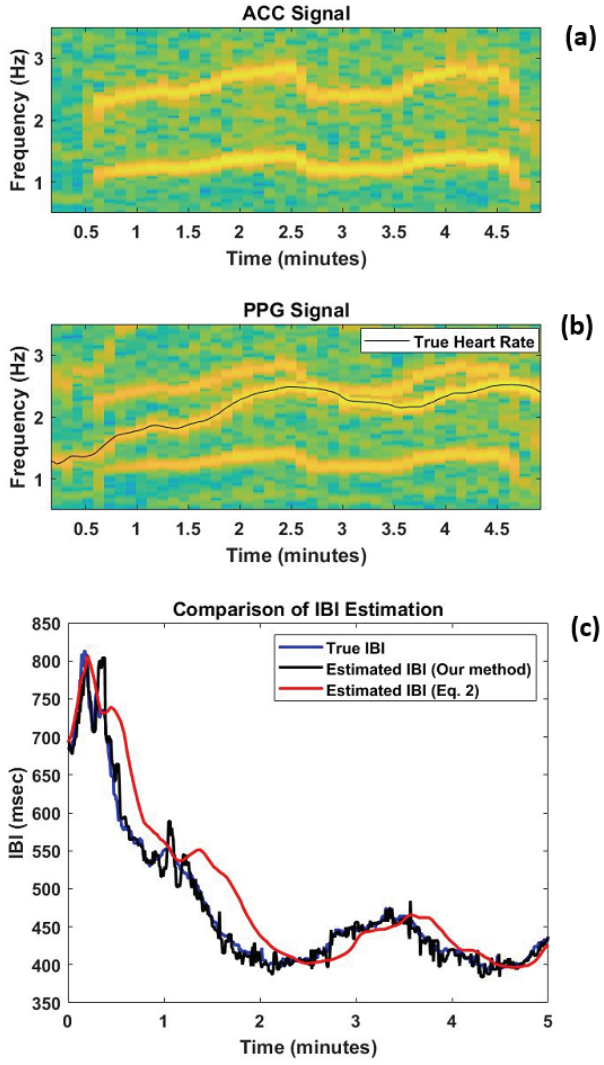

Fig. 8. IBI estimation performance for subject 9. (a) Spectrogram of original ACC signal, (b) spectrogram of original PPG signal with the true heart rate, (c) and the comparison of estimated IBI by using proposed fusion technique and the estimated IBI with the most rudimentary method defined in Eq. 2, and the true IBI obtained from clean ECG.

Heart Rate Variability Acquired from ECG

To test the performance of our technique in conjunction with HRV parameter estimation from noisy ECG signals, eight different HRV parameters are calculated at various SNR levels. Then, Pearson correlation coefficients between the estimated and true HRV parameters are calculated to illustrate how our technique provides an accurate estimation of HRV in the presence of various motion distortion levels. Table IV provides the correlations of eight different HRV parameters obtained from clean and noisy ECG signals for 12 subjects at various SNR levels where r represents the Pearson correlation coefficient. The estimated and true HRV parameters are highly correlated and most of the Pearson correlation coefficients are above 0.98 with the SNR levels of 6dB, 4dB, 2dB, and 0dB. Despite, some HRV parameters including STD HR, LF power, and HF power indicate relatively lower correlations when SNR level is -2dB, the results indicate that our technique provides a rigorous estimation of HRV parameters in the presence of various noise distortion levels. Moreover, Fig. 9 depicts the correlation plots of selected time domain HRV parameters including mean IBI and mean HR. Fig. 10 shows the correlation plots of selected frequency domain HRV parameters including LF power and VLF power all of which are obtained from noisy and clean ECG signals in the presence of different noise

TABLE IV
HRV RESULTS FOR NOISY ECG

HRV Parameters	*r* (6 dB)	*r* (4 dB)	*r* (2 dB)	*r* (0 dB)	*r* (-2 dB)
Mean RR (*ms*)	0.999 (<0.001)	0.999 (<0.001)	0.999 (<0.001)	0.999 (<0.001)	0.998 (<0.001)
SDNN (*ms*)	0.997 (<0.001)	0.998 (<0.001)	0.993 (<0.001)	0.990 (<0.001)	0.970 (<0.001)
Mean HR (*1/min*)	0.999 (<0.001)	0.999 (<0.001)	0.999 (<0.001)	0.999 (<0.001)	0.999 (<0.001)
STD. HR (*1/min*)	0.996 (<0.001)	0.997 (<0.001)	0.997 (<0.001)	0.975 (<0.001)	0.954 (<0.001)
LF Power (ms^2)	0.978 (<0.001)	0.950 (<0.001)	0.859 (<0.001)	0.814 (<0.002)	0.613 (<0.03)
HF Power (ms^2)	0.950 (<0.001)	0.978 (<0.001)	0.863 (<0.002)	0.814 (<0.002)	0.746 (<0.01)
VLF Power (ms^2)	0.999 (<0.001)	0.999 (<0.001)	0.998 (<0.001)	0.996 (<0.001)	0.976 (<0.001)
Total Power (ms^2)	0.998 (<0.001)	0.995 (<0.001)	0.988 (<0.001)	0.984 (<0.001)	0.886 (<0.001)

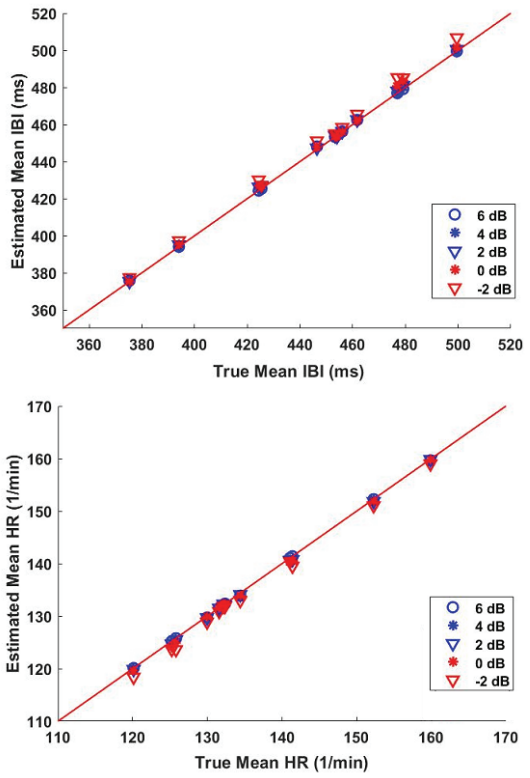

Fig. 9. Correlations of time-domain HRV parameters mean HR and mean IBI obtained from noisy ECG in the presence of different SNR levels: 6dB, 4dB, 2dB, 0dB, and -2dB.

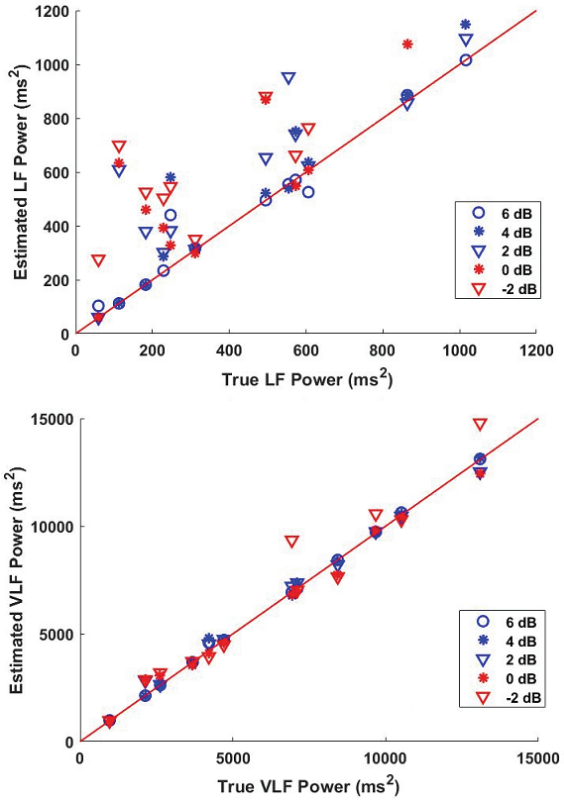

Fig. 10. Correlations of frequency-domain HRV parameters LF power and VLF power obtained from noisy ECG in the presence of different SNR levels: 6dB, 4dB, 2dB, 0dB, and -2dB.

distortion levels. The correlation plots indicate high correlations even with intense noise levels.

There have been relatively few methods on IBI and HRV estimation in the presence of intense physical activities due to the fact that this field of study is rather new. Hence, we further assess the HRV estimation performance of our proposed technique on ECG signals by comparing our results with the artifact detection and correction method proposed by Lipponen et. al. [26] and illustrate the results in Table V in various SNR levels. The results indicate that despite both techniques provide an accurate estimation of HRV parameters in relatively higher SNR values, our proposed technique provides a better HRV estimation performance in the presence of intense noise distortion levels.

Heart Rate Variability Acquired from Fusion of PPG Features

We test the robustness of the fusion of multiple morphological features in detecting the HRV parameters from noisy PPG signals. We calculate the average Pearson correlation coefficients between the estimated and true HRV parameters for 12 subjects where the results are illustrated in Table VI. We observe that almost all of the estimated HRV parameters are highly correlated with the ground truth where most of the correlation coefficients hover 0.90 or above. However, the HF components have relatively lower values compared to the rest of HRV parameters where HF values, obtained from PPG, were reported as noticeably over-estimated compared to the HF components obtained from ECG in the presence of intense physical exercise which is the possible reason of the comparatively lower values [45].

TABLE VI
HRV RESULTS FOR NOISY PPG

HRV Parameters	*r*
Mean RR (*ms*)	0.9861 (<0.001)
SDNN (*ms*)	0.9555 (<0.001)
Mean HR (*1/min*)	0.9871 (<0.001)
STD. HR (*1/min*)	0.8603 (<0.001)
LF Power (ms^2)	0.8984 (<0.01)
HF Power (ms^2)	0.8284 (<0.05)
VLF Power (ms^2)	0.9814 (<0.001)
Total Power (ms^2)	0.9736 (<0.001)

D. Problem Complexity

In Algorithm I which presents the shortest path calculation, the main *for* loop runs N times for N vertices while the inner loop runs m steps, where m represents the number of former vertices of any vertex. Since the former vertices are selected from a bounded window, m is assumed to be constant. In light of this observation, we define the complexity of Algorithm I as $O(N)$. While we increase the window size, the complexity of the algorithm increases linearly, and in an extreme case it turns into $O(N^2)$ if the window size is close to the entire signal duration. Due to the nature of the problem, we would prefer to choose the window size close to average IBI which turns the complexity of the problem to $O(N)$.

In Algorithm II, which illustrates the fusion technique of numerous morphological features, the first *for* loop runs for p times, which is the number of segments, while the second loop

contains n steps, which is the number of samples inside any segment. As $n \cong N/p$, in extreme case where all of the morphological features are estimated as true heartbeats, the complexity of Algorithm II becomes $O(N)$.

E. Discussion

The IBI estimation results obtained from noisy ECG signals show that the estimated IBI arrays are highly correlated with the ground truth in the presence of various noise levels. The performance is acceptable even with -2dB SNR level and the correlation coefficients are greater than 0.92 for the SNR levels of 6dB, 4dB, and 2dB. However, the IBI estimation performance is decreased significantly when the SNR level is decreased to -2dB due to the fact that the average HR estimation error, which directly affects the performance of our technique, is also increased. Moreover, The IBI estimation results for noisy PPG signals indicate that the performance is improved when multiple features are used. The correlation results offer better performance in the case of using any of the two morphological features together while the highest performance is achieved when all three morphological features are used. The performance is expected to further increase if additional morphological features are leveraged. We further demonstrate that our method accurately estimates different HRV parameters from noisy ECG in the presence of various motion distortion levels. Moreover, we establish that different HRV parameters are calculated accurately from noisy PPG signals, in particular when all three morphological features are used.

Sampling rate is another aspect for our HRV analysis. Some of the previous studies use higher sampling rates such as 1 kHz [24] where some others utilize relatively lower sampling rates such as 196 Hz [46]. We upsampled our data to 500 Hz by considering that this value is sufficient enough to capture the IBI and HRV where the power of the pulse signals is predominated between 0-10 Hz [21] and most of the signal components exist below 250 Hz. We also consider the further development of wearable sensors for IBI and HRV estimation where the data storage is an important consideration which guides the selection of the sampling rate of 500 Hz.

Despite, our proposed techniques accurately estimate IBI and HRV parameters, there are some limitations. One is the dependence of our algorithm on the accurate estimation of average HR values which could be obtained by any state-of-the-art methods. When the performance of the average HR detection algorithm is degraded, the performance of our technique is decreased. In the future work, we will improve our technique by reducing reliance on average HR. Another limitation is the dataset that we used for evaluation. We used the SP Cup 2015 dataset which contains 12 healthy subjects. As this dataset contains two-channel motion-corrupted PPG signals and clean ECG signals recorded simultaneously, it provides a suitable evaluation platform. However, we did not test our technique on datasets that include abnormal cardiac signals and irregular heartbeats such as arrhythmias or atrial fibrillation. Furthermore, we evaluated our proposed techniques on one-channel physiological signal modalities. However, an array of physiological signals, which are recorded simultaneously, might further improve the estimation of IBI and HRV parameters. In future, we will extend our technique to multi-channel signals which are recorded simultaneously.

VI. Conclusion

In this work, we proposed a combinatorial algorithm, based on shortest path, to detect true IBIs from the morphological features of ECG and PPG signals in the presence of motion artifact. Systolic peaks, maximum slopes, and onsets were detected as the pronounced and characteristics components of PPG signals while R-peaks are explored as the most important characteristic point of ECG signals for robust estimation of IBI and HRV. A fusion technique was introduced to leverage different morphological features of one-channel physiological signal modality. Our results indicated that the estimated IBI arrays obtained from noisy ECG are highly correlated with the ground truth even in the presence of intense motion corruptions. In the case of noisy PPG, the mean of the correlation coefficients appeared around 0.89 when all morphological features are used. We demonstrated that the fusion technique can be extended to various morphological features to enhance the performance of IBI and HRV estimation. Moreover, most of the estimated HRV parameters from noisy ECG and PPG signals offer high correlations compared to the ground truth. Additionally, the shortest path exploration problem can be applied to different physiological signal modalities such as bio-impedance for the robust estimation of IBI and HRV in the presence of motion artifacts.

Acknowledgment

This work was supported, in part by the National Institutes of Health, under grant 1R01EB028106-01, and the National Science Foundation, under grants CNS-1738293 and EEC-1648451. Any opinions, findings, conclusions, or recommendations expressed in this material are those of the authors and do not necessarily reflect the views of the funding organizations.

References

[1] D. L. Mann, D. P. Zipes, P. Libby and R. O. Bonow, Braunwald's Heart Disease E-Book: A Textbook of Cardiovascular Medicine, *Elsevier Health Sciences*, 2014.

[2] C. J. McAloon, L. M. Boylan, T. Hamborg, N. Stallard, F. Osman, P. B. Lim and S. A. Hayat, "The changing face of cardiovascular disease 2000--2012: An analysis of the world health organisation global health estimates data," *International journal of cardiology*, vol. 224, pp. 256-264, 2016.

[3] P. Kakria, N. Tripathi and P. Kitipawang, "A real-time health monitoring system for remote cardiac patients using smartphone and wearable sensors," *International journal of telemedicine and applications*, vol. 2015, pp. 1-11, 2015.

[4] J. Achten and A. E. Jeukendrup, "Heart rate monitoring," *Sports medicine*, vol. 33, no. 7, pp. 517-538, 2003.

[5] U. R. Acharya, K. P. Joseph, N. Kannathal, C. M. Lim and J. S. Suri, "Heart rate variability: a review," *Medical and biological engineering and computing*, vol. 44, no. 12, pp. 1031-1051, 2006.

[6] R. Mccraty and F. Shaffer, "Heart rate variability: new perspectives on physiological mechanisms, assessment of self-regulatory

capacity, and health risk," *Global advances in health and medicine*, vol. 4, no. 1, pp. 46-61, 2015.

[7] H. Cohen and J. Benjamin, "Power spectrum analysis and cardiovascular morbidity in anxiety disorders," *Autonomic Neuroscience*, vol. 128, no. 1-2, pp. 1-8, 2006.

[8] J. Parak, A. Tarniceriu, P. Renevey, M. Bertschi, R. Delgado-Gonzalo and I. Korhonen, "Evaluation of the beat-to-beat detection accuracy of PulseOn wearable optical heart rate monitor," in 37th Annual *International Conference of the IEEE Engineering in Medicine and Biology Society (EMBC)*, 2015.

[9] K. Georgiou, A. V. Larentzakis, N. N. Khamis, G. I. Alsuhaibani, Y. A. Alaska and E. J. Giallafos, "Can wearable devices accurately measure heart rate variability? A systematic review," *Folia medica*, vol. 60, no. 1, pp. 7-20, 2018.

[10] M. R. Ram, K. V. Madhav, E. H. Krishna, N. R. Komalla and K. A. Reddy, "A novel approach for motion artifact reduction in PPG signals based on AS-LMS adaptive filter," *IEEE Transactions on Instrumentation and Measurement*, vol. 61, no. 5, pp. 1445-1457, 2012.

[11] G. Cennini, J. Arguel, K. Aksit and A. Van Leest, "Heart rate monitoring via remote photoplethysmography with motion artifacts reduction," *Optics express*, vol. 18, no. 5, pp. 4867-4875, 2010.

[12] V. Nathan and R. Jafari, "Particle Filtering and Sensor Fusion for Robust Heart Rate Monitoring Using Wearable Sensors," *IEEE journal of biomedical and health informatics*, vol. 22, no. 6, pp. 1834-1846, 2018.

[13] Z. Zhang, Z. Pi and B. Liu, "TROIKA: A general framework for heart rate monitoring using wrist-type photoplethysmographic signals during intensive physical exercise," *IEEE Transactions on biomedical engineering*, vol. 62, no. 2, pp. 522-531, 2015.

[14] E. Khan, F. Al Hossain, S. Z. Uddin, S. K. Alam and M. K. Hasan, "A robust heart rate monitoring scheme using photoplethysmographic signals corrupted by intense motion artifacts," *IEEE Transactions on Biomedical engineering*, vol. 63, no. 3, pp. 550-562, 2016.

[15] K. T. Sweeney, T. E. Ward and S. F. McLoone, "Artifact removal in physiological signals—Practices and possibilities," *IEEE transactions on information technology in biomedicine*, vol. 16, no. 3, pp. 488-500, 2012.

[16] Sel, K., Zhao, J., Ibrahim, B., & Jafari, R. (2019). Measurement of Chest Physiological Signals using Wirelessly Coupled Bio-Impedance Patches. *2019 41st Annual International Conference of the IEEE Engineering in Medicine and Biology Society (EMBC)* (pp. 376--381). IEEE.

[17] T. Sakamoto, R. Imasaka, H. Taki, T. Sato, M. Yoshioka, K. Inoue, T. Fukuda and H. Sakai, "Feature-Based Correlation and Topological Similarity for Interbeat Interval Estimation Using Ultrawideband Radar," *IEEE Transactions on Biomedical Engineering*, vol. 63, no. 4, pp. 747-757, 2015.

[18] X. Sun, P. Yang, Y. Li, Z. Gao and Y.-T. Zhang, "Robust heart beat detection from photo plethysmography interlaced with motion artifacts based on Empirical Mode Decomposition," *in IEEE-EMBS International Conference on Biomedical and Health Informatics*, Hong Kong and Shenzhen, 2012.

[19] T. V. Tran and W.-Y. Chung, "A robust algorithm for real-time peak detection of photoplethysmograms using a personal computer mouse," *IEEE Sensors Journal*, vol. 15, no. 8, pp. 4651-4659, 2015.

[20] R.-Y. Huang and L.-R. Dung, "Measurement of heart rate variability using off-the-shelf smart phones," *Biomedical engineering online*, vol. 15, no. 1, 2016.

[21] R.-C. Peng, X.-L. Zhou, W.-H. Lin and Y.-T. Zhang, "Extraction of heart rate variability from smartphone photoplethysmograms," *Computational and mathematical methods in medicine*, vol. 2015, 2015.

[22] D. J. Rebergen, S. B. Nagaraj, E. S. Rosenthal, M. T. Bianchi, M. J. van Putten and M. B. Westover, "ADARRI: a novel method to detect spurious R-peaks in the electrocardiogram for heart rate variability analysis in the intensive care unit," *Journal of clinical monitoring and computing*, vol. 32, no. 1, pp. 53-61, 2018.

[23] J. M. Ahn, "Heart Rate Variability (HRV) analysis using simultaneous handgrip electrocardiogram and fingertip photoplethysmogram," *Advances in Information Sciences and Service Sciences*, vol. 5, no. 13, pp. 164-170, 2013.

[24] N. Selvaraj, A. Jaryal, J. Santhosh, K. K. Deepak and S. Anand, "Assessment of heart rate variability derived from finger-tip photoplethysmography as compared to electrocardiography," *Journal of medical engineering & technology*, vol. 32, no. 6, pp. 479--484, 2008.

[25] B. Vescio, M. Salsone, A. Gambardella and A. Quattrone, "Comparison between electrocardiographic and earlobe pulse photoplethysmographic detection for evaluating heart rate variability in healthy subjects in short-and long-term recordings," *Sensors,* vol. 18, no. 3, p. 844, 2018.

[26] Lipponen, J., & Tarvainen, M. (2019). A robust algorithm for heart rate variability time series artefact correction using novel beat classification. *Journal of medical engineering & technology,* 43(3), 173--181.

[27] Aygun, A., & Jafari, R. (2019). Robust Heart Rate Variability and Interbeat Interval Detection Algorithm in the Presence of Motion Artifacts. *2019 IEEE EMBS International Conference on Biomedical & Health Informatics (BHI)* (pp. 1--5). IEEE.

[28] Jankovic, D., & Stojanovic, R. (2017). Flexible system for HRV analysis using PPG signal. *In CMBEBIH 2017* (pp. 705--712). Springer.

[29] Sasikala, P., & Wahidabanu, R. (2010). Robust r peak and qrs detection in electrocardiogram using wavelet transform. *International Journal of Advanced Computer Science and Applications-IJACSA*, 1(6), 48--53.

[30] M. Elgendi, "On the analysis of fingertip photoplethysmogram signals," *Current cardiology reviews*, vol. 8, no. 1, pp. 14--25, 2012.

[31] Sviridova, N., & Sakai, K. (2015). Human photoplethysmogram: new insight into chaotic characteristics. *Chaos, Solitons & Fractals*, 77, 53--63.

[32] Kuntamalla, S., & Reddy, L. (2014). An efficient and automatic systolic peak detection algorithm for photoplethysmographic signals. *International Journal of Computer Applications*, 97(19).

[33] Yoon, Y., Cho, J., & Yoon, G. (2009). Non-constrained blood pressure monitoring using ECG and PPG for personal healthcare. *Journal of medical systems*, 33(4), 261--266.

[34] Rabbani, H., Mahjoob, M., Farahabadi, E., & Farahabadi, A. (2011). R peak detection in electrocardiogram signal based on an optimal combination of wavelet transform, hilbert transform, and adaptive thresholding. *Journal of medical signals and sensors*, 1(2), 91.

[35] Posada-Quintero, H., Delisle-Rodriguez, D., Cuadra-Sanz, M., & de la Vara-Prieto, R. (2013). Evaluation of pulse rate variability obtained by the pulse onsets of the photoplethysmographic signal. *Physiological measurement*, 34(2), 179.

[36] Ibrahim, B., & Jafari, R. (2019). Cuffless Blood Pressure Monitoring from an Array of Wrist Bio-impedance Sensors using Subject-Specific Regression Models: Proof of Concept. *IEEE transactions on biomedical circuits and systems.*

[37] M. Elgendi, Y. Liang and R. Ward, "Toward generating more diagnostic features from photoplethysmogram waveforms," *Diseases*, vol. 6, no. 1, p. 20, 2018.

[38] Mitchell, G., Pfeffer, M., Finn, P., & Pfeffer, J. (1997). Comparison of techniques for measuring pulse-wave velocity in the rat. *Journal of Applied Physiology*, 82(1), 203--210.

[39] A. Savitzky and M. J. Golay, "Smoothing and differentiation of data by simplified least squares procedures.," *Analytical chemistry*, vol. 36, no. 8, pp. 1627--1639, 1964.

[40] A. L. Goldberger, L. A. Amaral, L. Glass, J. M. Hausdorff, P. C. Ivanov, R. G. Mark, J. E. Mietus, G. B. Moody, C.-K. Peng and H. E. Stanley, "PhysioBank, PhysioToolkit, and PhysioNet: components of a new research resource for complex physiologic signals," *Circulation*, vol. 101, no. 23, pp. e215--e220, 2000.

[41] G. B. Moody, W. Muldrow and R. G. Mark, "A noise stress test for arrhythmia detectors," *Computers in cardiology*, vol. 11, no. 3, pp. 381--384, 1984.

[42] M. I. Davila, G. F. Lewis and S. W. Porges, "The Physiocam: a novel non-contact sensor to Measure heart rate Variability in clinical and Field applications," *Frontiers in public health,* vol. 5, p. 300, 2017.

[43] M. P. Tarvainen, J.-P. Niskanen, J. A. Lipponen, P. O. Ranta-Aho and P. A. Karjalainen, "Kubios HRV--heart rate variability analysis software," *Computer methods and programs in biomedicine,* vol. 113, no. 1, pp. 210-220, 2014.

[44] Berntson, G., Thomas Bigger Jr, J., Eckberg, D., Grossman, P., Kaufmann, P., Malik, M., . . . Stone, P. (1997). Heart rate variability: origins, methods, and interpretive caveats. *Psychophysiology*, 34(6), 623--648.

[45] Charlot, K., Cornolo, J., Brugniaux, J., Richalet, J.-P., & Pichon, A. (2009). Interchangeability between heart rate and photoplethysmography variabilities during sympathetic stimulations. *Physiological measurement*, 30(12), 1357.

[46] Bolanos, M., Nazeran, H., & Haltiwanger, E. (2006). Comparison of heart rate variability signal features derived from electrocardiography and photoplethysmography in healthy individuals. *2006 International Conference of the IEEE Engineering in Medicine and Biology Society* (pp. 4289--4294). IEEE.

Ayca Aygun is a Ph.D. student in Electrical Engineering at Texas A&M University. She received her B.S. degree in Mathematical Engineering and M.S. degree in Biomedical Engineering, both are from Istanbul Technical University in 2010 and 2015, respectively. She is currently working as a research assistant in Embedded Signal Processing Lab at Texas A&M University. Her research interests include biomedical signal processing, time series analysis, and statistical analysis.

Hassan Ghasemzadeh received the B.Sc. degree from the Sharif University of Technology, Tehran, Iran, in 1998, the M.Sc. degree from the University of Tehran, Tehran, in 2001, and the Ph.D. degree from The University of Texas at Dallas, Richardson, TX, USA, in 2010, all in computer engineering. He was a Faculty Member with Azad University from 2003 to 2006, where he was the Founding Chair of the Computer Science and Engineering Department, Damavand Branch, Tehran. He was a Post-Doctoral Fellow with the West Wireless Health Institute, La Jolla, CA, USA, from 2010 to 2011, and a Research Manager with the UCLA Wireless Health Institute from 2011 to 2013. He is currently an Assistant Professor of Computer Science with the School of Electrical Engineering and Computer Science, Washington State University, Pullman, WA, USA. His research focuses on algorithm design, machine learning, and system-level optimization for embedded and pervasive systems.

Roozbeh Jafari (SM'12) is an associate professor in Biomedical Engineering, Computer Science and Engineering and Electrical and Computer Engineering at Texas A&M University. He received his Ph.D. in Computer Science from UCLA and completed a postdoctoral fellowship at UC-Berkeley. His research interest lies in the area of wearable computer design and signal processing. His research has been funded by the NSF, NIH, DoD (TATRC), AFRL, AFOSR, DARPA, SRC and industry (Texas Instruments, Tektronix, Samsung & Telecom Italia). He has published over 100 papers in refereed journals and conferences. He has served as the general chair and technical program committee chair for several flagship conferences in the area of Wearable Computers. He is the recipient of the NSF CAREER award in 2012, IEEE Real-Time & Embedded Technology & Applications Symposium (RTAS) best paper award in 2011 and Andrew P. Sage best transactions paper award from IEEE Systems, Man and Cybernetics Society in 2014. He is an associate editor for the *IEEE Transactions on Biomedical Circuits and Systems, IEEE Sensors Journal, IEEE Internet of Things Journal* and *IEEE Journal of Biomedical and Health Informatics*. He serves on scientific panels for funding agencies frequently and is presently serving as a standing member of the NIH Biomedical Computing and Health Informatics study section.